Original scientific paper

FAST DOA ESTIMATION OF THE SIGNAL RECEIVED BY TEXTILE WEARABLE ANTENNA ARRAY BASED ON ANN MODEL[*]

Zoran Stanković, Olivera Pronić-Rančić, Nebojša Dončov

University of Niš, Faculty of Electronic Engineering, Niš, Serbia

Abstract. *MLP_DoA module, being an integral part of the smart TWAA DoA subsystem, intended for fast DoA estimation is proposed. Multilayer perceptron network is used to create the MLP_DoA module that provides a radio gateway location in azimuthal plane at its output when a spatial correlation matrix, found by receiving the radio gateway signal using two-element textile wearable antenna array, is on its input. MLP_DoA network training with monitoring the generalization capabilities on the validation set of samples is applied. The accuracy of the proposed modeling approach is compared to the classical approach in MLP_DoA module training previously developed by the authors. Comparison of the presented ANN model with the root MUSIC algorithm in terms of accuracy and program execution time is also done.*

Key words: *ANN, MLP, DoA, TWAA, root MUSIC*

1. INTRODUCTION

Wearable wireless systems play an integral role in the fifth generation (5G) networks, which operate with higher bit rates, lower latency, and lower outage probabilities in smaller microcells and picocells covering broader areas than 4G or older technologies. In addition, beam reconfigurability and beamforming are expected to facilitate spectral and energy efficiency at both the mobile devices and base station levels. Besides mobile communications, wearable wireless systems find numerous applications in areas such as health-care, security, ambient assisted leaving, sports etc., [2]-[7].

Wearable antennas are among the most important elements of wearable wireless systems, [8]-[15]. They are usually integrated within the clothing by any of current state-of-the-art fabrication methods (fabric-based embroidered antennas, polymer-embedded antennas, microfluidic antennas with injection alloys, inkjet printing, screen printing and photolithography, 3D-printed antennas, etc.) [9]. Depending on the type of application, it

is vital to choose a suitable antenna form, as one-design-fits-all approach often does not meet all requirements.

In health care monitoring (HCM), wireless technology enables a significant reduction in the cost of health services, while at the same time providing the necessary quality of service. Combination of biosensors placed on patient's body and antennas integrated into garments to transmit/receive signals to the remote wireless monitor point can allow the patients to receive the needed assistance, while continuing to live in their own homes [15].

A single textile wearable antenna with an omnidirectional radiation pattern is commonly used in health care monitoring systems. It allows to avoid signal level fluctuations between the antenna and a radio gateway (RG) of the HCM system due to wearer movements. However, the range of the single antenna is significantly reduced both outdoors and indoors due to its small gain. The classic antenna arrays provide significantly higher gain but have narrow and spatially invariant radiation patterns and therefore cannot overcome the problem of signal fluctuations due to the movement of antenna wearer. Textile wearable antenna arrays (TWAA) with adaptive beamforming (smart TWAA), on the other hand, provide that the main lobe of the antenna array radiation pattern is always directed towards the RG [15].

Direction-of-arrival (DoA) estimation of RG signal represents a crucial factor in adaptive beamforming [16]. Usually, DoA estimation requires intensive matrix calculations as it is based on super resolution algorithms such as MUSIC, ESPRIT, and their modifications. Therefore, their real-time implementation requires powerful hardware platforms, [17-20], which makes them unsuitable for implementation on small mobile platforms used to realise smart TWAA.

On the other hand, artificial neural networks (ANNs) for DoA estimation do not require complex matrix calculations and can be easily implemented on modest mobile hardware platforms, [21]-[26]. Further, from our previous research, it was shown that they have approximately the same modelling accuracy as super resolution algorithms, but significantly higher calculation speed [1], [24]-[26].

This paper is a continuation of the research presented in [1] where the basic version of the DoA module based on the MultiLayer Perceptron (MLP) network (MLP_DoA module) was proposed. That module is an integral part of the smart TWAA DoA subsystem with two textile antennas that performs fast DoA estimation of the RG signals and determination of the RG location in the azimuthal plane. The research conducted within this paper relates to further development and improvement of the MLP_DoA module as well as to the examination of its performances in a working environment having a wide range of signal-to-noise ratio changes. Unlike the classical approach in MLP_DoA module training, applied in [1], that did not include mechanisms of control of the achieved generalization capabilities of MLP network, in this paper, network training with monitoring the generalization capabilities on the validation set of samples and thus preventing the effect of its overlearning is applied. The proposed ANN approach in DoA estimation of the RG signal is compared with the classical approach in DoA estimation based on the root MUSIC algorithm in terms of accuracy and program execution time.

The paper is organized as follows. After Introduction, a brief description of the proposed smart TWAA DoA subsystem is given in Section 2. The architecture, training, and testing of MLP_DoA network are presented in Section 3. The most illustrative numerical results are presented in Section 4, and finally conclusion remarks are given in Section 5.

In order to facilitate interpretation of the material presented in these sections, the list of used acronyms is given in Table 1.

Table 1 List of used acronyms

A term replaced by its acronym (acronym)	
health care monitoring (HCM)	mean square error (MSE)
radio gateway (RG)	maximum validation failures (MVF)
textile wearable antenna arrays (TWAA)	worst case error (WCE)
direction-of-arrival (DoA)	average test error (ATE)
artificial neural networks (ANNs)	Pearson Product Moment correlation coefficient (r^{PPM})
multilayer perceptron (MLP)	signal-to-noise ratio (SNR)

2. SMART TWAA DOA SUBSYSTEM

Architecture of the smart TWAA DoA subsystem is shown in Fig. 1. It consists of two-element TWAA, narrowband filters, A/D convertors, FPGA module and DoA module. The distance between the antenna elements is $d = c/2f$, where c is the speed of light. TWAA, filters and A/D convertors perform the RG signal sampling at frequency f. Based on the samples provided by TWAA, FPGA module calculates the spatial correlation matrix (C). This matrix is then sent to the input of DoA module that determines the azimuth positions of the radio gateway (θ). ANNs are proposed for the realization of the DoA module (ANN based DoA module).
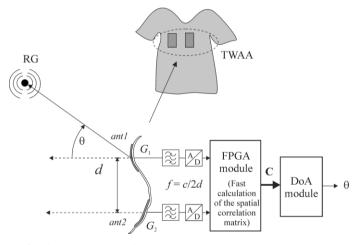

Fig. 1 Architecture of the smart TWAA DoA subsystem [1]

In the absence of the antenna noise, the vector of signals induced on TWAA with elements having omnidirectional radiation pattern in the azimuth plane is $x_s(t) = [x_{s1}(t) \; x_{s2}(t)]$, where $x_{s1}(t)$ and $x_{s2}(t)$ are the signals induced on the first and second antenna element, respectively. Accordingly, the correlation matrix of signals induced on elements can be expressed as [16]

$$\mathbf{C}_s = E[\mathbf{x}_s(t)\mathbf{x}_s^{\mathrm{H}}(t)] = p\mathbf{s}\mathbf{s}^H = \begin{bmatrix} p & pe^{-j\beta d \sin\theta} \\ pe^{j\beta d \sin\theta} & p \end{bmatrix} \tag{1}$$

where E [·] denotes expectation operator, s = [1 $e^{j\beta d\sin\theta}$]$^{\mathrm{T}}$ is the steering vector, β is the phase constant ($\beta=2\pi/\lambda$), and p is the power of the signal induced on one omnidirectional antenna element.

In the initial state, when the TWAA wearer does not move and the textile is not deformed, the gains of antenna elements are mutually equal, $G(\theta)=G_1(\theta)=G_2(\theta)$. In the general case, the TWAA wearer moves, the textile deformations occur and consequently there are changes in the orientation of the antenna elements and in their effective apertures. Therefore, the gains of antenna elements in the direction of the RG change over time and in general case, they can have different values at the same moment

$$G_1 = G_1(\theta,t) \neq G_2 = G_2(\theta,t), \quad \text{for most } t \text{ values} \tag{2}$$

Here, we assume that creasing of textile does not lead to a significant change in the distance between the antenna elements, i.e., this change can be neglected. Therefore, the equation (1), defining the correlation matrix of the signals received by the mobile TWAA, must be modified as follows

$$\mathbf{C}_s = \begin{bmatrix} G_1 p & \sqrt{G_1 G_2}\, pe^{-j\beta d\sin\theta} \\ \sqrt{G_1 G_2}\, pe^{j\beta d\sin\theta} & G_2 p \end{bmatrix}. \tag{3}$$

When the antenna noise is present and there is not any external RG signal, the noise vector induced on the antenna elements can be represented as n(t) = [$n_1(t)$ $n_2(t)$], where $n_1(t)$ and $n_2(t)$ are random noise components on the first and second antenna element, respectively. For uncorrelated noise, e.g., white Gaussian noise, the noise correlation matrix is obtained as

$$\mathbf{C}_n = E\,[\mathbf{n}(t)\mathbf{n}^{\mathrm{H}}(t)] = \begin{bmatrix} \sigma_n^2 & 0 \\ 0 & \sigma_n^2 \end{bmatrix}. \tag{4}$$

The spatial correlation matrix at the TWAA output, $\mathbf{C}$, can be obtained as a superposition of the correlation matrix of signals and the noise correlation matrix,

$$\mathbf{C} = E\,[\mathbf{x}(t)\mathbf{x}^{\mathrm{H}}(t)] =$$
$$= \mathbf{C}_s + \mathbf{C}_n = \begin{bmatrix} G_1 p + \sigma_n^2 & \sqrt{G_1 G_2}\, pe^{-j\beta d\sin\theta} \\ \sqrt{G_1 G_2}\, pe^{j\beta d\sin\theta} & G_2 p + \sigma_n^2 \end{bmatrix} \tag{5}$$

where x(t) = x$_s$(t)+n(t) is the vector at the TWAA output.

The signal-to-noise ratio (*SNR*) is defined with respect to the power of the signal received by the first element of the antenna array,

$$SNR = \frac{G_1 p}{\sigma_n^2}. \tag{6}$$

Therefore, equation (5) can be expressed as follows

$$\mathbf{C} = \begin{bmatrix} G_1 p + \dfrac{G_1 p}{SNR} & \sqrt{G_1 G_2}\, p e^{-j\beta d \sin\theta} \\[2ex] \sqrt{G_1 G_2}\, p e^{j\beta d \sin\theta} & G_2 p + \dfrac{G_1 p}{SNR} \end{bmatrix}.$$

(7)

Normalization of the matrix $\mathbf{C}$ does not lead to a change in the results obtained by MUSIC algorithm for DoA estimation, [25]. By normalizing the matrix $\mathbf{C}$ with respect to element C_{11}, it is obtained that normalized matrix, $\mathbf{C'}$, is invariant to the signal strength p and for its determination is not necessary to know the gains of both antennas but only their relative ratio G_2/G_1,

$$\mathbf{C'} = \begin{bmatrix} 1 & \sqrt{\dfrac{G_2}{G_1}} \cdot \dfrac{SNR}{SNR+1} e^{-j\beta d \sin\theta} \\[2ex] \sqrt{\dfrac{G_2}{G_1}} \cdot \dfrac{SNR}{SNR+1} e^{j\beta d \sin\theta} & \dfrac{SNR}{SNR+1}\left(\dfrac{G_2}{G_1} + \dfrac{1}{SNR}\right) \end{bmatrix}$$

(8)

With the introduction of the variables: g (root gain ratio), $g = \sqrt{G_2/G_1}$, and the distance between antenna elements expressed in wavelengths, d_λ, Eq. (8) becomes

$$\mathbf{C'} = \begin{bmatrix} 1 & g \cdot \dfrac{SNR}{SNR+1} e^{-j2\pi d_\lambda \sin\theta} \\[2ex] g \cdot \dfrac{SNR}{SNR+1} e^{j2\pi d_\lambda \sin\theta} & \dfrac{SNR}{SNR+1}\left(g^2 + \dfrac{1}{SNR}\right) \end{bmatrix}$$

(9)

In the real scenario, the TWAA wearer moves, and the textile is crumpled, so it is exceedingly difficult to determine the parameters g and SNR at each time point. Also, the angle θ is unknown, so the spatial correlation matrix cannot be determined directly by applying the above formula. The spatial correlation matrix is estimated from a large number of TWAA output samples in a short time interval (TWAA snapshots) using fast A/D converters and calculating the matrix elements on the FPGA module using the approximate formula

$$\mathbf{C} \approx \frac{1}{N_s} \sum_{s=1}^{N_s} \mathbf{x}_s \mathbf{x}_s^H ,$$

(10)

where x_s is the sample of s-th snapshot at TWAA output and N_s is the number of snapshots. An example of a measuring point and the necessary laboratory equipment for obtaining the elements of a correlation matrix by measurement are presented in [26].

3. ANN BASED DoA MODULE

The ANN based DoA module consists of a single MLP neural network (MLP_DoA) that estimates the angle of arrival of the RG signal on the TWAA based on the signal information contained in the spatial correlation matrix. This can be represented as follows

$$\theta = f_{MLP\_DoA}(\mathbf{C}') \,. \tag{11}$$

The first row of a normalized spatial correlation matrix without autocorrelation element is sufficient for estimating the angular positions of EM radiation sources, [1], [25]. The real and the imaginary part of the elements in the first row without the autocorrelation element, are brought separately to the neurons in the input layer of the MLP network. In this way, a model is obtained that is more suitable for implementation and training in relation to the case when the complex values of these elements are taken at the input of the MLP network, [23]. Accordingly, for the two-element TWAA, Eq. (11) can be written in the form

$$\theta = f_{MLP\_DoA}(\mathbf{c}) = f_{MLP\_DoA}(\mathrm{Re}\{C'_{12}\}, \mathrm{Im}\{C'_{12}\}) \,, \tag{12}$$

where $\mathbf{c}$ is the vector of the input variables of the MLP neural network ($\mathbf{c} = [\mathrm{Re}\{C_{12}'\}$ $\mathrm{Im}\{C_{12}'\}]$.)

3.1. Architecture of MLP_DoA network

The architecture of MLP_DoA network is shown in Fig. 2. It consists of a total of L layers of neurons: one input and one output layer of neurons and a total of L-2 hidden layers of neurons between them.
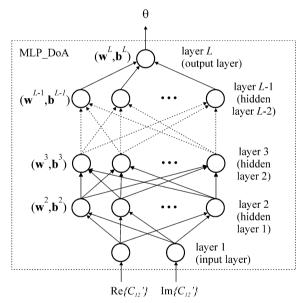

Fig. 2 Architecture of MLP_DoA network.

The signal propagation from the input to the output of the MLP network and the corresponding transfer functions of the MLP_DoA network (Eq. 12) can be described by the output vectors of each network layer. The input layer is a buffer layer and, according to Eq. (12), has two neurons. Thus, the output vector of the input layer is $\mathbf{y}^1 = \mathbf{c} = [\mathrm{Re}\{C_{12}'\}$ $\mathrm{Im}\{C_{12}'\}]$. The output vector of l-th layer (except the input layer) can be expressed as

$$\mathbf{y}^l = F_l(\mathbf{w}^l \mathbf{y}^{l-1} + \mathbf{b}^l) \quad l = 2,3,\ldots,L \tag{13}$$

where $\mathbf{y}^{l-1}$ represents the output of $(l$-1)-th layer. In Eq. (13), $\mathbf{w}^l$ is the connection weight matrix between the $(l$-1)-th and the l-th layer where matrix element $w^l_{i,j}$ represents the connection weight between the j-th neuron of the $(l$-1)-th layer and the i-th neuron of the l-th layer, $\mathbf{b}^l$ is the vector containing biases of the l-th layer where vector element b^l_i represents bias of the i-th neuron of the l-th layer, while $F_l(\cdot)$ is an activation function of l-th layer neurons. The hyperbolic tangent sigmoid transfer function was used as an activation function of hidden layers

$$F_l(u) = \frac{e^u - e^{-u}}{e^u + e^{-u}} \quad , \quad l = 2,3,\ldots,L-1 . \tag{14}$$

The output layer has one neuron with the linear activation function $F_L(u) = u$ and its output is given as

$$\theta = \mathbf{y}^L = F_L(\mathbf{w}^L \mathbf{y}^{L-1} + \mathbf{b}^L) = \mathbf{w}^L \mathbf{y}^{L-1} + \mathbf{b}^L . \tag{15}$$

The weight matrices $\mathbf{w}^1$, $\mathbf{w}^2,\ldots, \mathbf{w}^L$, and bias vectors $\mathbf{b}^1$, $\mathbf{b}^2,\ldots, \mathbf{b}^L$ form the set W of the trainable parameters of the MLP network. The values of the elements of this set are adjusted during the network training with the aim that the mapping expressed by Eq.(12) is realized with the desired accuracy.

The general architecture of this MLP_DoA neural network is represented by the notation MLPH-N_1-$\ldots$-N_i-$\ldots$-N_H. H and N_i in this notation are the total number of hidden layers in MLP architecture ($H = L$-2) and the total number of neurons in the i-th hidden layer, respectively.

3.2. Training and testing of MLP_DoA network

MLP_DoA network training is performed on a set of training samples $P = \{(\mathbf{c}_1,\theta_1^D),$ $(\mathbf{c}_2,\theta_2^D),\ldots, (\mathbf{c}_s,\theta_s^D),\ldots,(\mathbf{c}_{Np},\theta_{Np}^D)\}$, where θ_s^D is the desired value of the network output when the sample $\mathbf{c}_s$ is brought to its input and N_P is the total number of training samples. To monitor the achieved degree of the network generalization, the validation set V, containing the total number of N_V samples of the same format as the samples of the training set P, is applied. During the network training, the samples from the training set are brought to the network input and an iterative change of weights and biases from the set W is performed in accordance with the chosen training algorithm. The goal is to minimize the mean square error (MSE) of the network output relative to the desired output values. Regarding the observation of network performance at the training set, the network training is stopped either when the target MSE at the training set ($E_{Ptarget}$) is reached or if the maximum number of iterations, N_{Imax}, is reached. During the network training, the MSE of the network output at the validation set, $E_V(W)$, is also monitored and when its minimum value (E_{Vmin}) is reached, the training is stopped, even if the above conditions for termination of the network training are not met. In fact, when E_{Vmin} is achieved, any further training of the MLP_DoA network leads to the network overfitting and deterioration of its generalization abilities. In other words, this means that the problem of finding the optimal breakpoint of the neural network training comes down to

finding the values of network weights and biases from the set *W* for which the network will have a minimum mean square error at the validation set (Eq. 16).

$$E_{V \min}(W) = \min_{W} \left(\frac{1}{2N_V} \sum_{s=1}^{N_V} (\theta_s - \theta_s^D)^2 \right) \tag{16}$$

If during the iterative training of the MLP_DoA network is noticed that the error at the validation set after a period of continuous decline begins to grow in the next *MVF* (*maximum validation failures*) successive iterations, then it is considered that the minimum error has been reached and the training should be stopped. The *MVF* value is set before the start of the network training. In the example of MLP_DoA network training that is presented in this paper, a test set intended for checking the generalization performance of the trained network was used as a validation set in the network training process (*V=T*).

Each sample used for neural network training or testing was obtained by establishing an inverse DoA mapping according to Eq. (9) and averaging a large number of consecutive TWAA snapshots according to Eq. (10). The training and test set of the samples contain ordered triplets of the format (Re{C′$_{12}$(θ^D[°], *g* [dB], *SNR* [dB])}, Im{C′$_{12}$(θ^D[°], *g* [dB], *SNR* [dB])}, θ^D [°]), where the samples are generated for different values of the angle θ^D and the parameter *g*.

The MLP_DoA network training set is generated by a uniform distribution of the variables θ^D and *g* as

$$P^{(SNR)} = \left\{ \begin{array}{l} (\text{Re}\{C'_{12}(\theta^D, g, SNR)\}, \text{Im}\{C'_{12}(\theta^D, g, SNR)\}, \theta^D)) \,| \\ \theta^D \in [\theta_{min}^D : \theta_{step}^D : \theta_{\max}^D], \, g \in [g_{min} : g_{step} : g_{\max}] \end{array} \right\} \tag{17}$$

where θ^D_{min}, θ^D_{step} and θ^D_{max} are the minimum value, step, and the maximum value of the angle θ^D, respectively, and g_{min}, g_{step} and g_{max} are the minimum value, step, and the maximum value of the parameter *g* in the training set, respectively.

In order to assess the quality of network training, the quality of generalization of the trained network and the final choice of MLP_DoA network architecture to be used for the implementation of DoA module, each trained network was tested on a test set that does not contain samples used in the training process. Similar to the training set, the test set was generated by a uniform distribution of the variables θ^D and g as

$$T^{(SNR)} = \left\{ \begin{array}{l} (\text{Re}\{C'_{12}(\theta^D, g, SNR)\}, \text{Im}\{C'_{12}(\theta^D, g, SNR)\}, \theta^D) \,| \\ \theta^D \in [\theta_{min}^{Dt} : \theta_{step}^{Dt} : \theta_{max}^{Dt}], \, g \in [g_{min}^{Dt} : g_{step}^{Dt} : g_{max}^{Dt}] \end{array} \right\} \tag{18}$$

where θ^{Dt}_{min}, θ^{Dt}_{step} and θ^{Dt}_{max} are the minimum value, step, and the maximum value of the angle θ^D in the test set, respectively, and g^t_{min}, g^t_{step} and g^t_{max} are the minimum value, step, and the maximum value of the parameter *g* in the test set, respectively.

The following metrics were used in the neural network testing process: worst case error (*WCE*), average test error (*ATE*) and Pearson product moment (PPM) correlation coefficient (r^{PPM}), [22]. Worst case error is calculated as

$$WCE = \max_{s=1}^{N_T} \left| \frac{\theta(\mathbf{c}_s, W) - \theta_s^D}{\theta_{\max}^D - \theta_{\min}^D} \right|, \tag{19}$$

where N_T is the total number of test set samples, $\theta(\mathbf{c}_s, W)$ is the output of MLP_DoA network when the sample $\mathbf{c}_s$ is brought to its input, and θ^D_{max} and θ^D_{min} are the maximum and minimum desired values of angle θ in test set, respectively.

Average test error is calculated as

$$ATE = \frac{1}{N_T} \sum_{s=1}^{N_T} \left| \frac{\theta(\mathbf{c}_s, W) - \theta^D_s}{\theta^D_{max} - \theta^D_{min}} \right|. \tag{20}$$

PPM correlation coefficient is calculated as

$$r^{PPM} = \frac{\sum_{s=1}^{N_T} (\theta(\mathbf{c}_s, W) - \bar{\theta}) \cdot (\theta^D_s - \bar{\theta}^D)}{\sqrt{\left[\sum_{s=1}^{N_T} (\theta(\mathbf{c}_s, W) - \bar{\theta})^2 \right] \cdot \left[\sum_{s=1}^{N_T} (\theta^D_s - \bar{\theta}^D)^2 \right]}}, \tag{21}$$

where $\bar{\theta} = \frac{1}{N_T} \sum_{s=1}^{N_T} \theta(\mathbf{c}_s, W)$ - represents the average value of neural network output and

$\bar{\theta}^D = \frac{1}{N_T} \sum_{s=1}^{N_T} \theta^D_s$ - represents the average value of expected output values.

4. MODELING RESULTS

Simulation of TWAA DoA subsystem operation, generation of training and testing samples, as well as development and testing of MLP_DoA modules were performed in MATLAB environment. The reference computer configuration used to implement DoA module and for all simulations was: Intel Core i7-9700F CPU @ 3 GHz, with 16 GB RAM. The following modeling scenario was considered: RG has radiation power of 1 W (0 dBW) and its distance from TWAA is 100m. TWAA wearer moves in the azimuth plane and its positions in relation to the RG change from -60° to +60°. As the wearer moves, textile creases, and the root gain ratio changes from -10 to 10 dB. The antenna elements are at a constant distance d_λ=0.5 and the number of snapshots is N_s=300.

For the development and testing of MLP_DoA module, training and test sets are formed using the Eqs. (17) and (18). The training set, $P^{(20)}$, is formed for SNR = 20 dB and test sets are formed for the following signal to noise ratio values: SNR$\in\{$20 dB, 15 dB, 10 dB, 5 dB, 0 dB, -5 dB$\}$ (denoted as $T^{(20)}$, $T^{(15)}$, $T^{(10)}$, $T^{(5)}$, $T^{(0)}$, $T^{(-5)}$). The following parameter values in the Eq. (17) were used to generate the training set: θ_{min} = -60°, θ_{step} = 0.5°, θ_{max} = 60°, g_{min} = -10 dB, g_{step} = 1dB and g_{max} = 10 dB. In this way, a training set containing 5061 samples was generated. The following parameter values in the Eq. (18) were used to generate the test set: θ^t_{min} = -60°, θ^t_{step} = 0.7°, θ^t_{max} = 60°, g^t_{min} = -10 dB, g^t_{step} = 1.3 dB, and g^t_{max} = 10 dB. In this way, 2752 samples were generated for each test set.

The development phase of the DoA module includes training and testing of a number of different MLP_DoA networks as well as selection of MLP network with the best test characteristics for the implementation of the DoA module. During this phase, it is

assumed that the antenna environment is almost ideal in terms of noise, the signal to noise ratio is SNR=20 dB. Therefore, the sets $P^{(20)}$ and $T^{(20)}$ were used to train and test different MLP_DoA networks. For the implementation of the MLP_DoA module, MLP architectures with two hidden layers ($H = 2$) and a variable number of neurons in them were considered. A number of different MLP networks having $N_1 \leq 8$ neurons and $N_2 \leq 22$ neurons were trained and tested.

Levenberg – Marquardt algorithm [22] was chosen to train MLP_DoA networks by tracking the achieved degree of network generalization at the validation set. During the training of the MLP_DoA networks, $T^{(20)}$ test set was used as a validation set. The following values of training parameters were selected: $E_{Ptarget} = 10^{-6}$, $N_{Imax} = 1000$ and $MVF = 20$.

Testing of all trained MLP_DoA networks was performed with the $T^{(20)}$ test set. Worst case error (*WCE*), average test error (*ATE*) and correlation coefficient (r^{PPM}) were monitored during the test procedure in order to find the MLP_DoA network capable of providing the angle of arrival of RG signal on the TWAA with the best accuracy.

Eight MLP_DoA networks that have the best test statistics are shown in Table 2. It can be seen that MLP2-18-16 neural network has the lowest values of *WCE* and *ATE* and the highest value of r^{PPM}. Therefore, this neural network was chosen for the implementation of the MLP_DoA module.

The test statistics obtained by the presented modelling approach are significantly better than the corresponding ones presented in [1] where the selected MLP_DoA module (MLP2-10-5) had the following statistics: *WCE*=2.7949, *ATE*=0.3699 and r^{PPM}=0.9998546. Namely, it is shown that approach in training and selection of the appropriate MLP network architecture for the realisation of MLP_DoA module presented here, significantly improves the accuracy of DoA estimation compared to the classical approach in MLP_DoA module training presented in [1].

The scattering diagram of the selected MLP2-18-16 neural network is shown in Fig. 3. In this case, a very high accuracy of DoA estimation can be observed.

Since the MLP network of MLP_DoA module was trained and tested in almost ideal noise conditions (*SNR*=20 dB), it was necessary to test the MLP_DoA module in case of an environment with increased noise in order to investigate the impact of noise on its accuracy. Therefore, the MLP_DoA module was tested in a noisy environment with a *SNR* of 15 dB, 10 dB, 5 dB, 0 dB, and -5 dB using $T^{(15)}$, $T^{(10)}$, $T^{(5)}$, $T^{(0)}$, and $T^{(-5)}$ test sets, respectively.

In order to compare the accuracy of the proposed ANN approach in DoA estimation of the RG signals with the classical approach based on super-resolution algorithms, the implementation of DoA module with the root MUSIC algorithm was performed (root MUSIC DoA module). Testing of the root MUSIC DoA module was performed under the same conditions and with the same test sets as in the case of the MLP_DoA module.

Table 2 Testing results for MLP_ANNs with the best test statistics

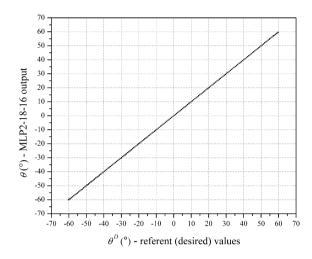| MLP_DoA network	WCE (%)	ATE (%)	r^{PPM}
MLP2-18-16	0.3466	0.0344	0.9999993
MLP2-14-11	0.3479	0.0432	0.9999980
MLP2-12-12	0.3735	0.0495	0.9999975
MLP2-15-11	0.3971	0.0596	0.9999964
MLP2-17-11	0.4368	0.0627	0.9999958
MLP2-22-10	0.4685	0.0488	0.9999974
MLP2-14-12	0.4837	0.0439	0.9999978
MLP2-14-11	0.5366	0.0571	0.9999965

Fig. 3 Scattering diagram of MLP2-18-16 neural network (*SNR* = 20 dB)

Based on the test results, the accuracy of both modules was examined and compared for different SNR values. The values of the worst case errors, average test errors and correlation coefficients obtained by the MLP_DoA module and by the root MUSIC DoA module versus signal-to-noise ratio are shown in Fig. 4 - 6. It is evident that both modules have very high accuracy in the case of low noise environment (*SNR*=20 dB, 15 dB, 10 dB). With increasing noise, i.e., decreasing *SNR*, there is a decrease in the accuracy of both modules, which becomes significant for *SNR* values less than 5 dB. However, in the case of increased noise, the proposed MLP_DoA module achieves better results.
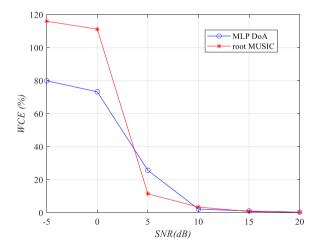

Fig. 4 Worst case error versus *SNR* obtained by MLP_DoA module and by the root MUSIC DoA module
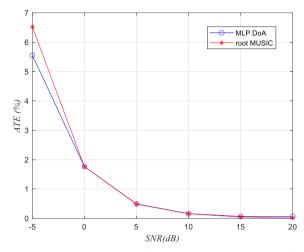
Fig. 5 Average test errors versus *SNR* obtained by MLP_DoA module and by the root MUSIC DoA module
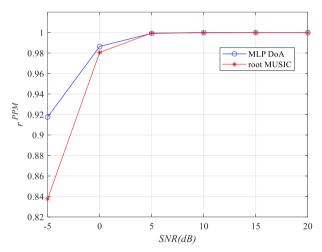

Fig. 6 *PPM* correlation coefficient obtained by MLP_DoA module and by the root MUSIC DoA module

The scattering diagram of both modules in case of extremely high noise, *SNR* = -5dB, are shown in Figs. 7 and 8. Fig. 7 shows the scattering diagram of the MLP_DoA module. In this case, the following test statistics were obtained: *WCE*=79.9515, *ATE*=5.5533 and r^{PPM}=0.9175. Fig. 8 shows the scattering diagram of root MUSIC DoA module. In this case, the following test statistics were obtained: *WCE*=116.0627, *ACE*=6.5200 and r^{PPM}=0.8376. Comparing the scattering diagrams of both modules, similar conclusions can be drawn as in the previous case. Both modules show significant deviation of the output values from the referent (desired) ones for a large number of samples, however, the scattering in the case of the MLP_DoA module is less than the scattering of the root MUSIC module, therefore, the MLP_DoA module shows less accuracy reduction in conditions of intense noise than the root MUSIC module.
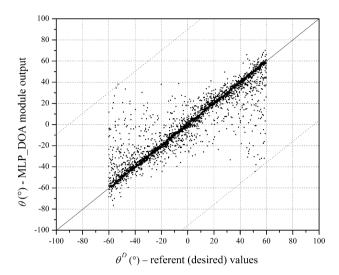
Fig. 7 Scattering diagram obtained by the MLP_DoA module in conditions with high noise level (*SNR* = -5 dB, solid line - line of ideal value matching, dashed lines - boundaries of the scattering area)

In addition, the average program execution time, measured on the test set with 2752 samples, for the MLP_DoA module is 0.008054 seconds and for the root MUSIC DoA module is 0.366337 seconds (Table 3). Obviously, the MLP based DoA module performs DoA estimation significantly faster compared to the root MUSIC DoA module (approximately 45 times faster).
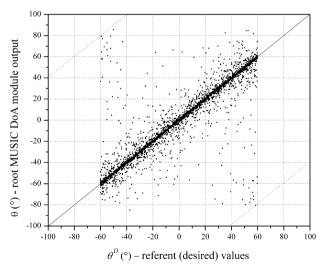

Fig. 8 Scattering diagram obtained by the root MUSIC DoA module in conditions with high noise level (*SNR* = -5 dB, solid line - line of ideal value matching, dashed lines - boundaries of the scattering area)

Table 3 Comparison of DoA estimation speed of the MLP_DOA module and the root MUSIC module measured on test set (Intel Core i7-9700F CPU @ 3 GHz, 16 GB RAM)

DoA module	Run time @ 2752 samples (s)
MLP_DoA module	0.008054
Root MUSIC DoA module	0.366337

5. CONCLUSION

An improved MLP_DoA module for fast DoA estimation of the RG signal arrival angle on two-element textile wearable antenna array has been proposed. The multilayer perceptron network, which was used to create this module, learned to accurately determine the position of the radio gateway in the azimuth plane from the spatial correlation matrix obtained by sampling the RG signal at TWAA. Since the classical approach in MLP_DoA module training, did not include mechanisms to control the achieved generalization capabilities of the MLP network, in this paper the training of MLP network was performed by monitoring the generalization capabilities on the validation set of samples. The obtained MLP_DoA module has an extremely high accuracy of DoA estimation in low noise conditions, i.e., better modelling accuracy was achieved compared to the results obtained by the classical approach in the training of the MLP_DoA module. In addition, the proposed module was compared with the root MUSIC algorithm in terms of accuracy and execution time of the program. The selected MLP_DoA module was shown to have approximately the same accuracy as the root MUSIC DoA module in the case of low noise conditions and less degradation of the model accuracy in a very noisy environment. Besides, MLP_DoA module performs DoA estimation approximately 45 times faster compared to the root MUSIC DoA module.

Creasing of textiles can cause the center frequencies of the antenna elements of TWAA to shift, as well as change the distance between the antenna elements. This leads to the effect of changing the phase difference of the signals received by the antennas regardless of the change in the angular position of the RG. This effect limits the accuracy of the MLP_DoA module. Therefore, further research will be aimed at increasing the accuracy of the MLP_DoA module by developing the methods to reduce this effect. One of the methods that will be applied is the training of MLP_DoA network with the samples of RG signals emitted at two different frequencies. Also, during further research, MLP_DoA module for TWAA with more than two antenna elements will be developed.

References

[1] Z. Stanković, O. Pronić-Rančić and N. Dončov, "ANN based DoA Estimation of the Signal Received by Two-element Textile Wearable Antenna Array", In Proceedings of the 15th International Conference on Advanced Technologies, Systems and Services in Telecommunications (TELSIKS), 2021, pp. 86-91.

[2] Cisco White paper, "Cisco Visual Networking Index: Global Mobile Data Traffic Forecast Update, 2016-2021 White Paper", March 2017.

[3] Z. Lin et al., "A low-power, wireless, real-time, wearable healthcare system", In Proceedings of the IEEE MTT-S International Wireless Symposium (IWS), 2016, pp. 1-4.

[4] T. Liang and Y. J. Yuan, "Wearable Medical Monitoring Systems Based on Wireless Networks: A Review," *IEEE Sensors J.*, vol. 16, no. 23, pp. 8186-8199, Dec. 2016.

[5] C. Lin et al., "Wireless and Wearable EEG System for Evaluating Driver Vigilance", *IEEE Trans. Biomed. Circuits Syst.*, vol. 8, no. 2, pp. 165-176, April 2014.

[6] V. Misra et al., "Flexible Technologies for Self-Powered Wearable Health and Environmental Sensing", *Proc. IEEE*, vol. 103, no. 4, pp. 665-681, April 2015.

[7] S. Saponara, "Wearable Biometric Performance Measurement System for Combat Sports", *IEEE Trans. Instrum. Meas.*, vol. 66, no. 10, pp. 2545-2555, Oct. 2017.

[8] N. F. M. Aun, P. J. Soh, A. A. Al-Hadi, M. F. Jamlos, G. A. E. Vandenbosch and D. Schreurs, "Revolutionizing wearables for 5G: 5G technologies: Recent developments and future perspectives for wearable devices and antennas", *IEEE Microw. Mag.*, vol. 18, no. 3, pp. 108-124, 2017.

[9] B. Mohamadzade, R. M. Hashmi, R. B. V. B. Simorangkir, R. Gharaei, S. Ur Rehman and Q. H. Abbasi, "Recent Advances on Fabrication Methods for Flexible Antennas in Wearable Devices: State of the Art", *Sensors*, vol. 19, no. 10, p. 2312, 2019.

[10] A. Sabban, "Small New Wearable Metamaterials Antennas for IoT, Medical and 5G Applications", In Proceedings of the 14th European Conference on Antennas and Propagation (EuCAP), 2020, pp. 1-5.

[11] H. Lee, J. Tak and J. Choi, "Wearable Antenna Integrated into Military Berets for Indoor/Outdoor Positioning System", *IEEE Antennas Wirel. Propag. Lett.*, vol. 16, pp. 1919-1922, 2017.

[12] S. M. Saeed, C. A. Balanis, C. R. Birtcher, A. C. Durgun and H. N. Shaman, "Wearable Flexible Reconfigurable Antenna Integrated with Artificial Magnetic Conductor", *IEEE Antennas Wirel. Propag. Lett.*, vol. 16, pp. 2396-2399, 2017.

[13] S. Su and Y. Hsieh, "Integrated Metal-Frame Antenna for Smartwatch Wearable Device", *IEEE Trans. Antennas Propag.*, vol. 63, no. 7, pp. 3301-3305, July 2015.

[14] M. Virili, H. Rogier, F. Alimenti, P. Mezzanotte and L. Roselli, "Wearable Textile Antenna Magnetically Coupled to Flexible Active Electronic Circuits", *IEEE Antennas Wirel. Propag. Lett.*, vol. 13, pp. 209-212, 2014.

[15] P. J. Soh et al., "A smart wearable textile array system for biomedical telemetry applications", *IEEE Trans. Microw. Theory Techn.*, vol. 61, no. 5, pp. 2253-2261, May 2013.

[16] L. C. Godara, "Application of antenna arrays to mobile communications, II: Beamforming and direction-of-arrival considerations", *Proc. IEEE*, vol. 85, pp. 1195-1245, 1997.

[17] M. I. Miller, and D. R. Fuhrmann, "Maximum likelihood narrow-band direction finding and the EM algorithm", *IEEE Trans. Acoust., Speech Signal Processing*, vol. 38, no. 9, pp. 1560-1577, 1990.

[18] R. Schmidt, "Multiple emitter location and signal parameter estimation", *IEEE Trans. Antennas Propag.*, vol. 34, no. 3, pp. 276-280, 1986.

[19] R. Roy and T. Kailath, "ESPRIT-estimation of signal parameters via rotational invariance techniques", *IEEE Trans. Acoust., Speech Signal Process*, vol. 37, no. 9, pp. 984-995, 1989.

[20] V. V. Reddy, M. Mubeen and B. Poh Ng, "Reduced-Complexity Super-Resolution DOA Estimation with Unknown Number of Sources". *IEEE Signal Process. Lett.*, vol. 22, no. 6, pp. 772-776, 2015.

[21] S. Haykin, *Neural Networks,* New York, IEEE Press, 1994.

[22] Q. J. Zhang and K. C. Gupta, *Neural networks for RF and microwave design*, Boston, Artech House, 2000.

[23] A. Hirose, *Complex-Valued Neural Networks: Advances and Applications*, Wiley, 2013.

[24] Z. Stanković, N. S. Dončov, I. Milovanović and B. Milovanović, "1D DoA Estimation of Mobile Stochastic EM Sources with a High Level of Correlation using MLP-based Neural Model", *Electromagnetics*, vol. 38, no. 8, pp. 500-516, 2018.

[25] Z. Stanković, N. Dončov, I. Milovanović, B. D. Milovanović, "DoA Estimation of Mobile Stochastic EM Sources with Variable Radiation Powers using Hierarchical Neural Model", *Int. J. RF Microwave Computer-Aided Eng.*, vol. 29, no. 10, p. e21901, pp. 1-17, 2019.

[26] M. Agatonović, Z. Stanković, I. Milovanovic, N. S. Dončov, L. Sit, T. Zwick, B. D. Milovanović, "Efficient Neural Network Approach for 2D DOA Estimation Based on Antenna Array Measurements", *Prog. Electromagn. Res., PIER 137*, vol. 137, pp. 741-758, 2013.